Phase-field model of solute trapping during solidification

A. A. Wheeler,* W. J. Boettinger, and G. B. McFadden
National Institute of Standards and Technology, Gaithersburg, Maryland 20899
(Received 14 September 1992)

A phase-field model for isothermal solidification of a binary alloy is developed that includes gradient energy contributions for the phase field and for the composition field. When the gradient energy coefficient for the phase field is smaller than that for the solute field, planar steady-state solutions exhibit a reduction in the segregation predicted in the liquid phase ahead of an advancing front (*solute trapping*), and, in the limit of high solidification speeds, predict alloy solidification with no redistribution of composition. Such situations are commonly observed experimentally.

PACS number(s): 64.70.Dv, 68.10.Gw, 81.30.Bx, 82.65.Dp

I. INTRODUCTION

Sharp-interface models of alloy solidification typically employ the solution to the usual diffusion equations for heat and solute in the bulk phases. The matching of solutions at the liquid-solid interface is obtained from flux conditions required for conservation and through constitutive laws for the jump in concentration across the interface and its temperature as functions of interface velocity. The latter are obtained from a separately derived model of the atomistics of solute diffusion across the interface. The dependence of the jump in concentration on velocity is termed *solute trapping* and provides a mechanism whereby the jump vanishes at high rates of solidification consistent with experimental observations (partitionless solidification). While this modeling approach has met with considerable success, it is clear that at high rates of solidification (1 $\mathrm{m\,s^{-1}}$) the concentration gradient near a freezing interface may be sufficiently large that gradient energy terms, as in the Cahn-Hilliard equation, should be included in the solute-diffusion problem in the liquid. The phase-field model presented in this paper will provide a common framework for the incorporation of these terms into the diffusion equation and at the same time provide a description of the diffusion in the interfacial zone, thus avoiding the requirement for separately derived constitutive laws for the interface conditions.

Kinetic theories for solute trapping fall into two categories, diffuse and sharp interface theories. Baker [1] solved the dilute-solution-continuum diffusion equation in a moving reference frame across a diffuse interface with various assumed spatial variations of energy to predict solute trapping by rapid growth. Langer and Sekerka [2] demonstrated that a solution to the Cahn-Hilliard equation in one dimension exhibits a reduction in the change in composition across a diffuse moving interfacial region between two phases as the velocity of the front increases. Their solution requires a miscibility gap (double-well potential) in the conserved order parameter (composition).

Many sharp interface theories of solute trapping are typified by the approach of Chernov [3]. Analytic and Monte Carlo models of trapping based on very similar principles to Chernov's have been developed by others [4–7]. In these models, an impurity atom must actively jump into the solid crystal at levels in excess of the equilibrium solubility. Thus special assumptions are required regarding preferential adsorption at the interface. In the approach of Aziz [8], the impurity may end up in the crystal on a high-energy site by virtue of the formation by its neighbors of a regular lattice around it. Hence to avoid incorporation onto a high-energy lattice site, an atom must diffuse away. Since the maximum speed of diffusion can be rather slow compared to the speed with which crystal-melt interfaces can move [9–11], the atom may be trapped on a high-energy site by a rapidly moving interface.

Phase-field models have been used to describe solidification of pure materials for many years. In this context they were developed by Langer [12, 13], Caginalp [14], and also Collins and Levine [15]. Caginalp has also extensively studied their mathematical properties [16, 17]. A recent review of phase-field models is given by Fife [18]. More recently, phase-field models that deal with alloy solidification have been developed by Lowen, Bechoefer, and Tuckerman [19] and Wheeler, Boettinger, and McFadden (WBM) [20].

In previous work [20], the authors have presented a phase-field model for *alloys* in which a free-energy surface and field equations were developed for the phase field $\phi(\mathbf{x},t)$ and the solute concentration $c(\mathbf{x},t)$. This work contained a gradient energy term for the phase field but not for the solute field. Asymptotic analysis of this model in the limit of a sharp interface, while recovering the required flux conditions based on conservation of solute at the interface as well as the Gibbs-Thomson effect for curved interfaces, produced a model in which the jump in concentration across the interfacial zone *increased* in magnitude as a function of velocity. This effect, which is contrary to experiments on solute trapping [21–23], is eliminated in the model presented in this paper. The essential feature that caused this difficulty was made evident by the *parallel* tangent condition that arises in the asymptotic analysis. This condition requires that the concentrations of the liquid and solid phases on the two sides of the interface must be given by two tangent points to the curves for the liquid and solid free-energy

 ©1993 The American Physical Society

density versus concentration, respectively. The two tangents must be parallel and separated by a energy that is an increasing function of the growth velocity. The parallel tangent condition precludes the possibility of solute trapping, since the resulting interfacial solid and liquid concentrations generally cannot approach each other. In this paper we will show that inclusion of the gradient-energy term for the solute breaks this condition and allows solute trapping to occur.

The incorporation of gradient-energy terms into the diffusion problem requires a gradient-energy coefficient not present in phase-field models for pure materials or in the previous model for alloys. This new coefficient, δ, affects the thickness of the thin solute transition zone between liquid and solid phases independent of the thickness of the phase-field transition zone, which is determined by the gradient-energy coefficient for the phase field, ε. Whereas the introduction of the phase field and its associated gradient-energy coefficient may be viewed as artificial and a regularization of the moving boundary problem, the need for a gradient-energy coefficient for solute to describe properly diffusion in finely spaced multilayers [24–26] and during spinodal decomposition [27] is well documented. It therefore makes sense to consider an asymptotic analysis for small values of the ratio ε/δ. This limit implies that the spatial extent of the structural disorder is small compared to the spatial extent of the composition variation across an interface. Through this asymptotic analysis, we derive a new set of governing equations that depend only on δ and that, through comparison to experiments, may provide a database for δ without requiring values for ε. In order to illustrate our model we therefore will show results for three values of δ added to the materials properties used for nickel-copper alloys developed in our previous model [20]. Further, from predictions of our model we describe experimental measurements that could be used to determine values for δ for alloy solidification.

The present model is for isothermal solidification, wherein heat flow is ignored and the temperature, and the composition of the liquid far from the interface, would be controlled parameters. For a steady state, the theory would then predict the velocity of the interface and the compositions in the interfacial zone. With this approach, constant-velocity planar solutions cannot be obtained except under special conditions. Experimentally, heat flow generally has the role of setting the interface velocity, as, for example, in directional solidification. Thus it is useful to consider the velocity and the liquid composition far from the interfacial region as being controlled while the self-consistent temperature and the interfacial compositions are determined by the theory. This approach allows us to directly inspect the behavior of the model as the solidification velocity is increased through constant-velocity planar solutions.

In Sec. II we develop the general phase-field model for alloys and give the governing equations. In Sec. III we study solutions that correspond to a stationary planar interface and we present the asymptotic analysis that yields information about surface tension and adsorption. In Sec. IV we extend this asymptotic analysis to the case of a planar interface freezing at constant velocity, and obtain a new set of governing equations, with solutions that exhibit solute trapping. In the last section we discuss our results and compare them to the Aziz model of solute trapping [8, 28].

II. THE MODEL

In our previous model [20], the Helmholtz free-energy functional was assumed to depend only upon the phase-field $\phi(\mathbf{x},t)$, its gradient $\nabla\phi(\mathbf{x},t)$, and the concentration $c(\mathbf{x},t)$. This model recovers the standard diffusion equation in the bulk phases. In the sharp-interface limit of this model, when a planar interface propagates with a constant velocity, the process of solute segregation at the interface results in a solute boundary layer forming adjacent to the interface with a length scale D/V, where D is the diffusivity of solute in the liquid and V is the interface velocity. As V increases the associated solute gradients become correspondingly large, and the length scale of the solute field diminishes. In fact, for a typical value of the solute diffusivity of 10^{-5} cm^2 s^{-1}, the length scale D/V of the solute field approaches atomic dimensions for velocities on the order of 100 cm s^{-1}, which is common in rapid solidification experiments. It is well known that continuum treatments of diffusion processes that occur on length scales approaching atomic dimensions typically require the inclusion of gradient-energy effects.

To remedy this shortcoming we generalize the Helmholtz free-energy functional, $\mathcal{F}$, used in the previous phase-field formulation to allow it to depend on $\nabla c(\mathbf{x},t)$. This, as we show below, results in the characteristic length of the solute profile at high interface velocities that is larger than D/V. This provides a solidification model that is valid to much higher interface velocities than those based on the classical diffusion equation. For an isothermal binary alloy with components A and B we put

$$\mathcal{F}=\int_\Omega\left\{f(\phi,c)+\frac{\varepsilon^2}{2}(\nabla\phi)^2+\frac{\delta^2}{2}(\nabla c)^2\right\}dV, \qquad (1)$$

where Ω is the volume occupied by the system, c is the concentration (mole fraction) of B, and $\varepsilon>0$ and $\delta>0$ are the coefficients of the phase-field and solute gradient energies, respectively. The simplest choice for the Helmholtz free-energy density $f(\phi,c)$ corresponds to an ideal solution and is identical to the one used previously [20], as given by

$$f(\phi,c)=cf_B(\phi)+(1-c)f_A(\phi)+\frac{RT}{v_m}[c\ln c+(1-c)\ln(1-c)], \qquad (2)$$

where R is the universal gas constant, T is the temperature of the system, which is a parameter in the isothermal problem, and v_m is the molar volume, which is assumed to be constant. The terms proportional to RT/v_m in this equation correspond to the contribution to the Helmholtz

free-energy density of the entropy of mixing of an ideal solution model. The functions $f_A(\phi)$ and $f_B(\phi)$ represent the Helmholtz free energies of the pure materials A and B, respectively, with corresponding melting points $T_M^{(A)}$ and $T_M^{(B)}$. The functions are given by double-well potentials with respect to ϕ. As in our earlier model, we employ the forms used by Kobayashi [29]:

$$f_A(\phi) = W_A \int_0^\phi p(p-1)[p - \tfrac{1}{2} - \beta_A(T)]dp, \tag{3}$$

$$f_B(\phi) = W_B \int_0^\phi p(p-1)[p - \tfrac{1}{2} - \beta_B(T)]dp, \tag{4}$$

where W_A and W_B are constants. We assume that $T_M^{(B)} < T < T_M^{(A)}$, and that $-1/2 < \beta_A(T) < 0 < \beta_B(T) < 1/2$ [see Eq. (19) below]. A more complex form of Eq. (2) might include energy of mixing terms proportional to $c(1-c)$.

We require that the governing equations ensure that the Helmholtz free-energy functional decreases monotonically in time, and that the total solute within the system is conserved. Simple postulates satisfying these requirements are

$$\frac{\partial \phi}{\partial t} = -M_1 \frac{\delta \mathcal{F}}{\delta \phi}, \tag{5}$$

$$\frac{\partial c}{\partial t} = \boldsymbol{\nabla} \cdot M_2 \left(c(1-c) \boldsymbol{\nabla} \frac{\delta \mathcal{F}}{\delta c} \right), \tag{6}$$

where

$$\frac{\delta \mathcal{F}}{\delta \phi} = \frac{\partial f}{\partial \phi} - \varepsilon^2 \boldsymbol{\nabla}^2 \phi,$$

and

$$\frac{\delta \mathcal{F}}{\delta c} = \frac{\partial f}{\partial c} - \delta^2 \boldsymbol{\nabla}^2 c.$$

The quantities M_1 and M_2 are positive, and may depend on c, ϕ and T. Allowing M_2 to depend on ϕ can provide for different solute mobilities in the liquid and solid phases. In the present work we take M_1 and M_2 to be constants. Appropriate boundary conditions for a finite volume Ω are

$$\frac{\partial \phi}{\partial n} = \frac{\partial c}{\partial n} = \frac{\partial (\boldsymbol{\nabla}^2 c)}{\partial n} = 0, \tag{7}$$

where $\mathbf{n}$ is the outward normal to the boundary of Ω.

It follows that the highest spatial derivatives that appear in the phase-field equation (5) are given by the Laplacian operator, whereas those for the solute concentration (6) with $\delta \neq 0$ are given by the spatial biharmonic operator. For $\delta = 0$, the highest spatial derivatives that appear in the solute equation are given by the Laplacian, with a diffusion coefficient given by [20]

$$D = M_2 \frac{RT}{v_m}. \tag{8}$$

Our aim here is to study the effect of interface velocity on the segregation at the interface when a solute gradient energy is included in the model. For simplicity we confine our attention to planar interfaces; nevertheless, this still provides a rather complicated situation, and so to proceed we consider first a stationary interface in which the relative effects of the two gradient-energy terms are revealed.

Our extension of the phase-field equations given by (5) and (6) may be viewed as generalized forms of the Cahn-Allen [30] and Cahn-Hilliard equations [31], respectively. They are coupled through the energy density $f = f(\phi, c)$. The Cahn-Allen equation describes the motion of antiphase boundaries in chemically ordered crystal [$f = f(\phi)$], and the Cahn-Hilliard equation describes spinodal decomposition [32] [with $f = f(c)$]; in both cases, the appropriate form for f is given by a double well in ϕ or c, respectively. In order for a single set of governing equations to treat the motion of the liquid-solid interface for alloys *and also* for pure materials, the double well in the free energy must exist with respect to ϕ. For the ideal solution model considered here, the free energy is convex in the variable c.

III. STATIONARY INTERFACE

We first consider the solute and phase fields due to a stationary planar solid-liquid interface situated in an infinite region, in which the far-field boundary conditions are given by $c \to c_{+\infty}$ and $\phi \to 0$ as $z \to \infty$, and $c \to c_{-\infty}$ and $\phi \to 1$ as $z \to -\infty$. We choose the origin $z = 0$ such that the liquid ($\phi = 0$) lies in the region $z > 0$, and the solid ($\phi = 1$) lies in the region $z < 0$. The aim is to determine $c_{+\infty}$ and $c_{-\infty}$, which represent the bulk concentrations in the liquid and solid, respectively, and to identify the characteristic length scales associated with the solute and phase fields in the interfacial zone.

The steady one-dimensional forms of the governing equations (5) and (6) are given by

$$-\varepsilon^2 \phi_{zz} + f_\phi = 0, \tag{9}$$

$$-\delta^2 c_{zz} + f_c = A, \tag{10}$$

where we have integrated the solute equation twice and employed the far-field conditions that c is bounded. The boundary conditions are

$$(\phi, c) \to \begin{cases} (1, c_{-\infty}) & \text{as } z \to -\infty, \quad (11) \\ (0, c_{+\infty}) & \text{as } z \to \infty. \quad (12) \end{cases}$$

Equations (9) and (10) are simply the Euler-Lagrange equations that minimize $\mathcal{F}$ subject to the constraint that the solute is conserved; A is then the corresponding Lagrange multiplier. WBM considered the case $\delta = 0$ and showed that the concentrations $c_{+\infty}$ and $c_{-\infty}$ were given by the *common* tangent construction to the free-energy densities in each phase, $f(0, c)$ and $f(1, c)$.

It is convenient to recast (9) and (10) in the form

$$\varepsilon^2 \phi_{zz} + F_\phi = 0, \tag{13}$$

$$\delta^2 c_{zz} + F_c = 0, \tag{14}$$

where

$$F(\phi, c) = Ac - f(\phi, c),$$

in which case it is clear that the associated Hamiltonian

$$H = \frac{\varepsilon^2}{2}(\phi_z)^2 + \frac{\delta^2}{2}(c_z)^2 + F,$$

is conserved. Here, the Hamiltonian describes motion of a particle in the potential field given by F, with the spatial variable z playing the role of time and the gradients ϕ_z and c_z playing the role of velocity components. It is convenient in the present context to retain the coefficients ε and δ in the Hamiltonian, rather than rescaling so that the coefficients are equal, as would normally be done in a classical description of particle dynamics.

Since in the far field the spatial gradients vanish, by comparing the values of the Hamiltonian as $z \to \pm\infty$ it follows that

$$F(1, c_{-\infty}) = F(0, c_{+\infty}), \tag{15}$$

and, from the solute equation, it similarly follows that

$$F_c(1, c_{-\infty}) = F_c(0, c_{+\infty}) = 0. \tag{16}$$

Additionally, it is required that $F_\phi(1, c_{-\infty}) = F_\phi(0, c_{+\infty}) = 0$, but this is automatically satisfied from the assumed form of the free energies f_A and f_B. Equations (15) and (16) determine the three unknown quantities $c_{-\infty}$, $c_{+\infty}$, and A, and can be rewritten in the form

$$\frac{f(0, c_{+\infty}) - f(1, c_{-\infty})}{c_{+\infty} - c_{-\infty}} = A = f_c(0, c_{+\infty}) = f_c(1, c_{-\infty}). \tag{17}$$

The identical conditions hold for the case $\delta = 0$ [20]; in both cases $c_{-\infty}$ and $c_{+\infty}$ are determined from the common tangent construction using the free energies $f(1, c)$ and $f(0, c)$ of the two phases. Thus for a *stationary* interface, the inclusion of the solute gradient energy does not disrupt the common tangent construction, which is important because any dynamical theory of solute trapping must recover the equilibrium conditions for a stationary interface. However, the inclusion of the solute gradient energy does affect the spatial structure of the solute and phase fields, as we discuss next. In Fig. 1 we show the phase diagram computed from the present model for the nickel-copper alloy database given in Ref. [20]. The loci of $c_{-\infty}$ and $c_{+\infty}$ as functions of temperature are called the solidus and liquidus, respectively.

Numerical integration of the governing equations for various values of ε/δ are shown in Fig. 2. It is apparent from this figure that as ε/δ decreases, the width of the phase-field transition diminishes compared to that of the solute field. This change in scale of the phase field relative to the solute field as ε/δ decreases is a result of the decreasing importance of the phase-field gradient energy relative to the solute gradient energy.

A. Asymptotic analysis for $\varepsilon/\delta \ll 1$

To investigate the behavior of the stationary interface in more detail, we consider an asymptotic analysis in the limit $\varepsilon/\delta \to 0$. We can roughly associate the two lengths

$$\ell_\varepsilon = \varepsilon\sqrt{\frac{v_m}{RT}}, \qquad \ell_\delta = \delta\sqrt{\frac{v_m}{RT}} \tag{18}$$

as being characteristic of the transitions layer thicknesses of the phase field and solute field, respectively. In addition to the characteristic lengths ℓ_ε and ℓ_δ, the free energy used in the phase-field model involves the energy densities W_A and W_B, as well as the dimensionless functions $\beta_A(T)$ and $\beta_B(T)$, which together determine the double-well structure of the free energies of pure compo-

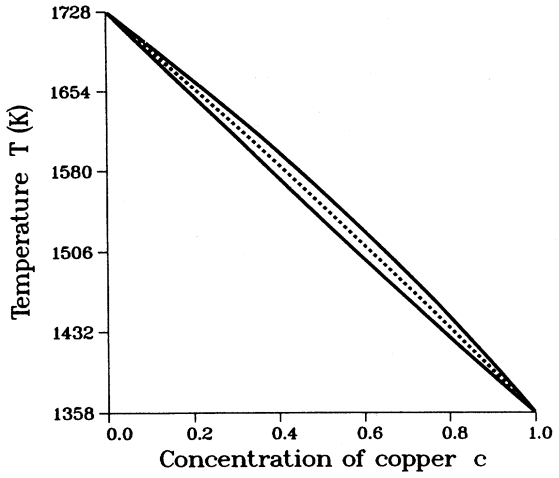

FIG. 1. The phase diagram for the nickel-copper alloy. The liquidus and solidus are represented by the upper and lower solid lines, respectively. They are computed from the common tangent construction (17). The dashed curve represents the quantity c^*, using the approximation $\Lambda = 0$ [see Eq. (35)].

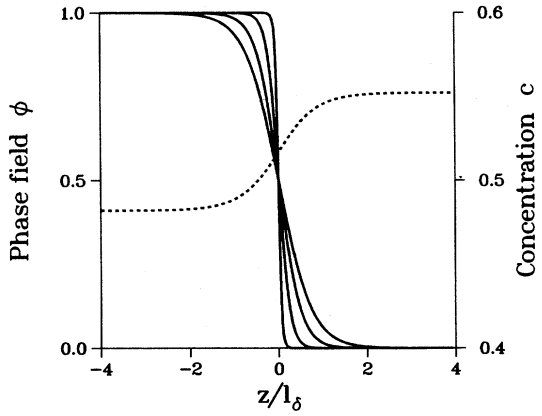

FIG. 2. Concentration (dashed line) and phase-field (solid line) profiles across a stationary interface obtained by numerical integration of Eqs. (9) and (10) for values of $(\varepsilon/\delta)^2$ of 0.01, 0.005, 0.002, and 0.0005. The smallest value corresponds to the sharpest profile for the phase field. The x axis is measured relative to $\ell_\delta = \delta\sqrt{v_m/RT}$; here $\delta = 3.3 \times 10^{-4}$ J$^{1/2}$ cm$^{-1/2}$ and $T = 1543$ K.

nent A and B in our model. We previously discussed how these quantities can be related to conventional material properties for solidification through the expressions [20]

$$\frac{W_A\beta_A(T)}{6} = L_A\frac{(T-T_M^{(A)})}{T_M^{(A)}}, \qquad \frac{W_B\beta_B(T)}{6} = L_B\frac{(T-T_M^{(B)})}{T_M^{(B)}}, \tag{19}$$

$$\sigma_A = \frac{\varepsilon\sqrt{W_A}}{6\sqrt{2}}, \qquad \sigma_B = \frac{\varepsilon\sqrt{W_B}}{6\sqrt{2}}, \tag{20}$$

where L_A and σ_A are the latent heat per unit volume and the surface tension, respectively, for pure component A, with the analogous definitions for component B. In performing the limit $\varepsilon/\delta \to 0$, it is also appropriate to scale the phase-field parameters W_A, W_B, β_A, and β_B in the appropriate fashion to maintain finite values of surface tension and latent heat as the phase-field transition layer becomes sharp relative to the solute layer.

To proceed we choose units based on the length ℓ_δ and energy density RT/v_m, and introduce the dimensionless variables $\tilde{z} = z/\ell_\delta$ and $\tilde{f} = f/[RT/v_m]$ (quantities with tildes will be dimensionless). We set $\tilde{\varepsilon} = \varepsilon/\delta$, and consider the limit $\tilde{\varepsilon} \to 0$. The scaled energy (2), on eliminating W_A and W_B in favor of σ_A and σ_B by using (19) and (20), then takes the form

$$\tilde{f}(\phi,c) = c\tilde{f}_B(\phi) + (1-c)\tilde{f}_A(\phi) + c\ln c + (1-c)\ln(1-c), \tag{21}$$

where

$$\tilde{f}_A(\phi) = \frac{1}{\tilde{\varepsilon}^2}\tilde{f}_A^{(-2)}(\phi) + \tilde{f}_A^{(0)}(\phi), \tag{22}$$

with

$$\tilde{f}_A^{(-2)}(\phi) = 18\tilde{\sigma}_A^2\phi^2(1-\phi)^2, \quad \tilde{f}_A^{(0)}(\phi) = \widetilde{\Delta F}_A\phi^2(3-2\phi), \tag{23}$$

and

$$\widetilde{\Delta F}_A = \frac{W_A\beta_A}{6[RT/v_m]} = \frac{L_A}{[RT/v_m]}\frac{(T-T_M^{(A)})}{T_M^{(A)}}, \qquad \frac{W_A}{[RT/v_m]} = \frac{72\tilde{\sigma}_A^2}{\tilde{\varepsilon}^2}.$$

Here $\widetilde{\Delta F}_A$, the dimensionless free-energy difference between the solid and liquid phases of pure A, and $\tilde{\sigma}_A = \sigma_A/(\delta\sqrt{RT/v_m})$, the dimensionless surface tension of pure A, are assumed to be of order unity in taking the limit. Similar definitions hold for the B component. We introduce the notation $\tilde{f}^{(n)} = c\tilde{f}_B^{(n)} + (1-c)\tilde{f}_A^{(n)}$ for $n = 0, -2$.

In the limit $\tilde{\varepsilon} \to 0$ it emerges that there are three different regions in $\tilde{z}$: one, which we refer to as the inner region, in which $\tilde{z}$ is small, and two others, which we refer to as the outer regions, where $\tilde{z}$ is of order unity; the latter regions are distinguished from one another by $\tilde{z}$ being positive or negative. We expand the solution in the outer regions as regular perturbation series in $\tilde{\varepsilon}^2$, i.e.,

$$\phi = \phi^{(0)}(\tilde{z}) + \tilde{\varepsilon}^2\phi^{(2)}(\tilde{z}) + O(\tilde{\varepsilon}^4),$$

and

$$c = c^{(0)}(\tilde{z}) + \tilde{\varepsilon}^2 c^{(2)}(\tilde{z}) + O(\tilde{\varepsilon}^4).$$

In the inner region we set $\tilde{z} = \tilde{\varepsilon}^2\tilde{x}$, and write similar expansions for the variables $\hat{c}(\tilde{x}) = c(\tilde{z})$, and $\hat{\phi}(\tilde{x}) = \phi(\tilde{z})$.

In the outer regions c varies but ϕ is effectively either zero or unity, and we find that, to all orders, $\phi = 0$ for $\tilde{z} > 0$ and $\phi = 1$ for $\tilde{z} < 0$. The leading-order problem for $c^{(0)}$ in the outer regions is then given by

$$-\frac{d^2c_-^{(0)}}{d\tilde{z}^2} + \tilde{f}_c(1, c_-^{(0)}) = \tilde{A} \quad \text{for } \tilde{z} < 0, \tag{24}$$

$$-\frac{d^2c_+^{(0)}}{d\tilde{z}^2} + \tilde{f}_c(0, c_+^{(0)}) = \tilde{A} \quad \text{for } \tilde{z} > 0, \tag{25}$$

where $\tilde{A} = A/[RT/v_m]$; note from Eq. (23) that the free energy $\tilde{f}(\phi,c)$ has no explicit $\tilde{\varepsilon}$-dependence when evaluated at $\phi = 0$ and $\phi = 1$. First integrals for these equations can be determined by integration with the far-field conditions $c_\pm^{(0)}(\tilde{z}) \to c_{\pm\infty}$ as $\tilde{z} \to \pm\infty$:

$$\frac{1}{2}\left(\frac{dc_-^{(0)}}{d\tilde{z}}\right)^2 - \tilde{f}(1, c_-^{(0)}) + \tilde{A}c_-^{(0)} = F_\infty \quad \text{for } \tilde{z} < 0, \tag{26}$$

$$\frac{1}{2}\left(\frac{dc_+^{(0)}}{d\tilde{z}}\right)^2 - \tilde{f}(0, c_+^{(0)}) + \tilde{A}c_+^{(0)} = F_\infty \quad \text{for } \tilde{z} > 0, \tag{27}$$

where $F_\infty = \tilde{A}c_{-\infty} - \tilde{f}(1, c_{-\infty}) = \tilde{A}c_{+\infty} - \tilde{f}(0, c_{+\infty})$, as follows from the common tangent conditions derived above.

Boundary conditions at the interface $\tilde{z} = 0$ are found by matching the solutions in the inner and outer regions. Expanding the expression $c(\tilde{z}) = c_+^{(0)}(\tilde{z}) + \tilde{\varepsilon}^2 c_+^{(2)}(\tilde{z}) + O(\tilde{\varepsilon}^4)$ for $\tilde{z} = \tilde{\varepsilon}^2\tilde{x}$ with $\tilde{z} > 0$ gives

$$c(\tilde{\varepsilon}^2\tilde{x}) = c_+^{(0)}(0) + \tilde{\varepsilon}^2\left(\frac{dc_+^{(0)}}{d\tilde{z}}(0)\tilde{x} + c_+^{(2)}(0)\right) + O(\tilde{\varepsilon}^4),$$

which provides the appropriate far-field boundary conditions for the solute field in the inner region for $\tilde{x} > 0$. Similar relations hold for $\tilde{z} < 0$.

To leading order the solution in the inner region satisfies

$$-\frac{d^2\hat{\phi}^{(0)}}{d\tilde{x}^2} + 72\left\{\tilde{\sigma}_B^2\hat{c}^{(0)} + \tilde{\sigma}_A^2[1-\hat{c}^{(0)}]\right\} \times\hat{\phi}^{(0)}(\hat{\phi}^{(0)}-1)(\hat{\phi}^{(0)}-\tfrac{1}{2}) = 0, \tag{28}$$

$$\frac{d^2\hat{c}^{(0)}}{d\tilde{x}^2} = 0. \tag{29}$$

The leading-order solute field is thus linear in the inner

region,

$$\hat{c}^{(0)}(\tilde{x}) = \hat{a}^{(0)}\tilde{x} + c^\star.$$

To match with the leading-order outer solution it must be a constant, $\hat{c}^{(0)}(\tilde{x}) = c^\star$. The value of $c^\star$, which we will call the interfacial concentration, is found through the matching procedure at next order. The leading-order phase field in the inner region is then found to have the explicit form

$$\hat{\phi}^{(0)}(\tilde{x}) = \tfrac{1}{2}[1 - \tanh(3\sigma^\star\tilde{x})], \tag{30}$$

where

$$\sigma^\star = \sqrt{c^\star\tilde{\sigma}_B^2 + (1-c^\star)\tilde{\sigma}_A^2} \tag{31}$$

is a dimensionless weighted average of the surface energies of the two components. This shows that the characteristic dimensional length associated with the phase field is actually $\tilde{\varepsilon}^2\ell_\delta/\sigma^\star$. The first-order problem is

$$-\frac{d^2\hat{\phi}^{(2)}}{d\tilde{x}^2} + \tilde{f}_{\phi\phi}^{(-2)}(\hat{\phi}^{(0)}, c^\star)\hat{\phi}^{(2)} + \tilde{f}_{c\phi}^{(-2)}(\hat{\phi}^{(0)}, c^\star)\hat{c}^{(2)} = -\tilde{f}_\phi^{(0)}(\hat{\phi}^{(0)}, c^\star), \tag{32}$$

$$-\frac{d^2\hat{c}^{(2)}}{d\tilde{x}^2} = -18(\phi^{(0)})^2(1-\phi^{(0)})^2[\tilde{\sigma}_B^2 - \tilde{\sigma}_A^2]. \tag{33}$$

This provides a solvability condition obtained by integrating Eq. (33), which after matching to the outer solution gives the following interfacial condition for the jump in the leading-order concentration gradient across the interfacial layer,

$$\left[\left.\frac{dc_+^{(0)}}{dz}\right|_{z=0^+} - \left.\frac{dc_-^{(0)}}{dz}\right|_{z=0^-}\right] = \Lambda, \tag{34}$$

where

$$\Lambda = \frac{\tilde{\sigma}_B^2 - \tilde{\sigma}_A^2}{2\sigma^\star}. \tag{35}$$

Employing Eqs. (26) and (27), we deduce that the interfacial concentration $c^\star$ is related to the interfacial concentration gradients at leading order by

$$\frac{\Lambda}{2}\left[\left.\frac{dc_-^{(0)}}{dz}\right|_{z=0^-} + \left.\frac{dc_+^{(0)}}{dz}\right|_{z=0^+}\right] = \tilde{f}^{(0)}(0,c^\star) - \tilde{f}^{(0)}(1,c^\star), \tag{36}$$

or

$$\frac{\Lambda}{\sqrt{2}}\left[\sqrt{F_\infty - F(1,c^\star)} + \sqrt{F_\infty - F(0,c^\star)}\right] = \tilde{f}^{(0)}(0,c^\star) - \tilde{f}^{(0)}(1,c^\star). \tag{37}$$

If $|\Lambda| \ll 1$, then Eq. (37) would be approximated by

$$\tilde{f}^{(0)}(0,c^\star) = \tilde{f}^{(0)}(1,c^\star), \tag{38}$$

and so $c^\star$ would be the concentration for which the Helmholtz free-energy density is continuous across the interface, and from Eq. (34), the derivative of the leading-order concentration would be continuous across the interfacial layer as well. The quantity Λ may be roughly estimated by $(\tilde{\sigma}_B - \tilde{\sigma}_A)/2$, which for a nickel-copper alloy [20] is given by $10^{-7}/\delta$, where δ has units $\mathrm{J}^{1/2}\ \mathrm{cm}^{-1/2}$. Below we illustrate the results of our model for three values of δ all greater than $3.3\times10^{-6}\ \mathrm{J}^{1/2}\mathrm{cm}^{-1/2}$, in which case $|\Lambda| \ll 3\times10^{-2}$ and so we expect this approximation to be reasonable. In the light of this, and for simplicity, in the remainder of the treatment of the stationary interface we will henceforth set $\Lambda = 0$, although incorporating the effects of nonzero values for Λ would present no essential difficulties.

We now summarize our findings under this assumption. The form of the free-energy function $f(\phi, c)$ determines the far-field values $c_{-\infty}$ and $c_{+\infty}$ through the common tangent construction (which does not depend on the value of Λ), and determines the constant value $c^\star$ of the leading-order concentration in the inner region. The leading-order phase field $\hat{\phi}^{(0)}(\tilde{x})$ in the inner region is given by Eq. (30), with far-field values given by $\hat{\phi}^{(0)} \to 1$ as $\tilde{x} \to -\infty$, and $\hat{\phi}^{(0)} \to 0$ as $\tilde{x} \to +\infty$. In the outer regions the leading-order concentration $c^{(0)}(\tilde{z})$ satisfies Eqs. (24) and (25) with $\phi^{(0)} = 0$ for $\tilde{z} > 0$ and $\phi^{(0)} = 1$ for $\tilde{z} < 0$. The far-field boundary conditions are $c_+^{(0)}(\tilde{z}) \to c_{+\infty}$ as $\tilde{z} \to \infty$ and $c_-^{(0)}(\tilde{z}) \to c_{-\infty}$ as $\tilde{z} \to -\infty$. At the origin the solute field and its derivative are continuous, and the solute concentration is given by $c^{(0)}(0) = c^\star$. The value of $c^\star$ is the concentration for which the Helmholtz free-energy density of the liquid and solid are equal. The dependence of $c^\star$ upon the temperature is shown in Fig. 1 by the dashed curve. [The curve $c^\star(T)$ is often referred to as the T_0 curve, [33]]. From this analysis we see that a complete separation of length scales of the solute and phase field occurs in the limit $\tilde{\varepsilon} \to 0$: the solute varies only in the outer region where $\tilde{z} = O(1)$, and the phase field varies only in the inner region where $\tilde{x} = O(1)$, and, to leading order, the transition from $\phi = 0$ to $\phi = 1$ is sharp on the length scale of the solute field.

B. Solute surface excess and surface tension

Solutions to the phase-field model with $\delta \neq 0$ provide an example where we can calculate the alloy surface tension and surface excess quantities associated with Gibb's notion of a diffuse interface [34]. In Gibbs' treatment, the system is assumed to consist of two bulk phases that are separated by a thin transition region whose thickness is small compared to the dimensions of the bulk sample. Outside of the transition region, each of the bulk phases is uniform, and the thermodynamic variables all assume equilibrium values appropriate to each phase. In the transition region there is a rapid but smooth change of the variables in passing from one phase to the other.

The diffuse transition region is then idealized by replacing this region by a dividing surface, located at some position within the transition region. Associated with the dividing surface are surface excess values of the ex-

tensive thermodynamic variables. In treatments of the thermodynamics of surfaces (see, for example, [35]), the alloy surface tension, σ, satisfies

$$\sigma = f_X - (\Gamma_A \bar{\mu}_A + \Gamma_B \bar{\mu}_B), \tag{39}$$

where f_X is the excess Helmholtz free energy per unit area of the dividing surface, Γ_A and Γ_B are the surface excess solute concentrations of components A and B, respectively, and $\bar{\mu}_A$ and $\bar{\mu}_B$ are the chemical potentials of components A and B, respectively. For a one-dimensional system with a stationary dividing surface located at $x = 0$ and with equal molar volumes v_m in each phase, the surface excess solute concentration Γ_B is defined by (see, for example, [36])

$$\int_{-L}^{L} c(z)\,dz = \int_{-L}^{0} c_S\,dz + \int_{0}^{L} c_L\,dz + v_m \Gamma_B,$$

where the interval of integration extends far enough into each bulk phase that the solute concentrations assume their bulk values in the liquid and solid, with $c(-L) = c_S$ and $c(L) = c_L$, with an analogous definition for Γ_A. It follows that for our model with equal molar volumes, we have $\Gamma_A = -\Gamma_B$. We note that the difference of the chemical potentials of the two components $(\bar{\mu}_B - \bar{\mu}_A)$ is given by $v_m A$, where A is the slope of the common tangent of the free-energy curves given in Eq. (17). The above expression (39) can then be written

$$\sigma = f_X - A v_m \Gamma_B. \tag{40}$$

The excess Helmholtz free energy per unit area associated with a planar interface that we use in our phase-field model is given by

$$f_X = \int_{-\infty}^{0} \left\{ [f(\phi, c) - f(1, c_{-\infty})] + \frac{\varepsilon^2}{2}\left(\frac{d\phi}{dz}\right)^2 + \frac{\delta^2}{2}\left(\frac{dc}{dz}\right)^2 \right\} dz + \int_{0}^{\infty} \left\{ [f(\phi, c) - f(0, c_{\infty})] + \frac{\varepsilon^2}{2}\left(\frac{d\phi}{dz}\right)^2 + \frac{\delta^2}{2}\left(\frac{dc}{dz}\right)^2 \right\} dz. \tag{41}$$

Employing the definition of $f(\phi, c)$, after some manipulation we obtain the expression

$$\sigma = \sigma_{[\phi]} + \sigma_{[c]}, \tag{42}$$

where

$$\sigma_{[\phi]} = \varepsilon^2 \int_{-\infty}^{\infty} \left(\frac{d\phi}{dz}\right)^2 dz$$

and

$$\sigma_{[c]} = \delta^2 \int_{-\infty}^{\infty} \left(\frac{dc}{dz}\right)^2 dz.$$

In the limit $\varepsilon/\delta \to 0$, it is natural to place the dividing surface at the position $z = 0$ where ϕ varies from zero to unity, since there is then no ambiguity about the interphase boundary location. Using the data for a nickel-copper alloy given in [20], Fig. 3 shows the leading-order expression for the surface excess of copper, defined by

$$v_m \Gamma_B = \int_{0}^{\infty} [c^{(0)}(z) - c_{+\infty}]dz + \int_{-\infty}^{0} [c^{(0)}(z) - c_{-\infty}]dz,$$

as a function of temperature between the two pure-component melting points.

The asymptotic analysis given above shows that to leading order $\sigma_{[\phi]}$ is the contribution to the surface tension associated with the inner layer where only ϕ changes and $\sigma_{[c]}$ is the contribution associated with the outer layers where c alone changes. These are given by

$$\sigma_{[\phi]} = \sqrt{c^* \sigma_B^2 + (1 - c^*)\sigma_A^2},$$

and

$$\sigma_{[c]} = \delta \sqrt{\frac{2RT}{v_m}} \left[\int_{c_{-\infty}}^{c^*} \sqrt{F(1, c)}\,dc + \int_{c^*}^{c_{+\infty}} \sqrt{F(0, c)}\,dc \right];$$

we note that $\sigma_{[\phi]}$ is the dimensional form of σ^*, and $\sigma_{[c]}$ is proportional to δ. The integrals must be evalu-

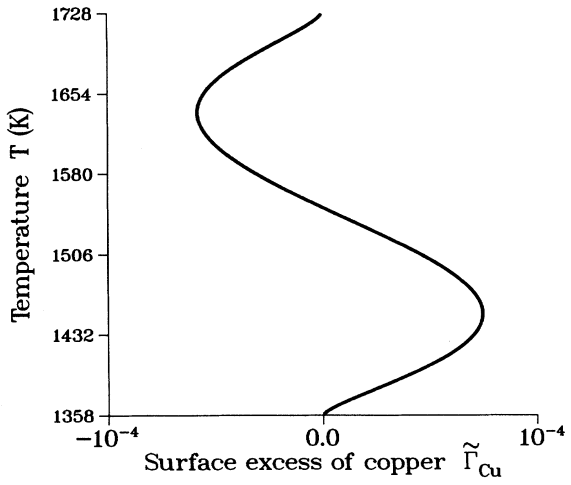

FIG. 3. The dimensionless surface excess of copper, $\tilde{\Gamma}_{Cu} = v_m \Gamma_{Cu}/\ell_\delta$, as a function of temperature between the melting points of pure nickel and pure copper, as computed from the leading-order terms in the asymptotic analysis.

ated numerically. From the definition of σ^* given by Eq. (31), and the dependence of c^* on temperature shown in Fig. 1, we see that $\sigma_{[\phi]}$ has a simple monotonic dependence on temperature, achieving the values of the pure two components at their melting points. In Fig. 4 we plot $\sigma_{[\phi]}$, $\sigma_{[c]}$, and σ as functions of temperature. The latter quantity is evaluated for three values of δ equal to 3.3×10^{-6} $J^{1/2}cm^{-1/2}$, 3.3×10^{-5} $J^{1/2}cm^{-1/2}$, and 3.3×10^{-4} $J^{1/2}cm^{-1/2}$. It is evident from the dependence of $\sigma_{[\phi]}$ and $\sigma_{[c]}$ on temperature that the surface tension of the interface, $\sigma = \sigma_{[\phi]} + \sigma_{[c]}$, may have at most a single maximum value, at a temperature between the melting temperatures of nickel and copper, and reduces to the value of the surface tension of either pure component at their melting points. The dependence of the surface tension upon temperature provides a way of determining the value of δ from experimental measurement.

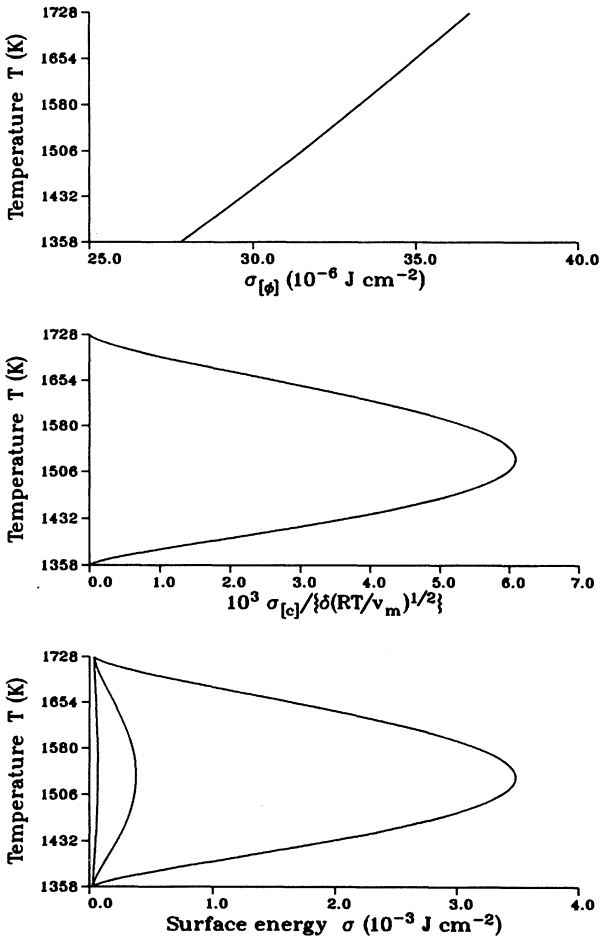

FIG. 4. The dimensional surface tension σ and its component parts $\sigma_{[\phi]}$ and $\sigma_{[c]}$ as functions of temperature, computed from the leading-order terms in the asymptotic analysis. The surface tension depends on δ and is plotted for three values of δ. The three curves in the lower diagram correspond (from left to right) to $\delta = 3.3 \times 10^{-6}$ $J^{1/2}cm^{-1/2}$, $\delta = 3.3 \times 10^{-5}$ $J^{1/2}cm^{-1/2}$, and 3.3×10^{-4} $J^{1/2}cm^{-1/2}$.

Few measurements of the dependence of alloy surface tension on temperature have been performed and these primarily for systems with limited solid solubility (see, for example, [37,38]). (Our assumption of an ideal solid solution provides for a full range of solid solubility.) Most of these systems show an increase in the liquid-solid surface tension with the addition of a solute which decreases the liquidus temperature, a trend recovered in the present model for the initial addition of component B to pure component A. Experimentally, the tension increases typically by no more than about 10% for a composition of 0.1. This suggests that the smallest values of δ used in Fig. 4 may be most appropriate.

An expression relating the temperature dependences of the adsorption and the surface tension may be derived in the Gibbs framework of surface excesses. This expression is beyond the scope of the present paper but its derivation involves the consideration of only those variations with temperature that maintain equilibrium between the liquid and solid phases as well as the interface. Qualitatively one knows that the surface adsorption adjusts itself to a value that lowers the surface tension. As temperature decreases, the composition (B content) of the bulk liquid and solid phases increases according to the phase diagram (Fig. 1). For an interface in a dilute alloy (high temperature and low B content) it can be seen from Fig. 4 that the surface tension increases as temperature decreases. Thus the surface tension can be thought of as increasing with composition. This requires that the surface should be lean in component B and thus have negative Γ_B, in agreement with Fig. 3 for high temperatures. At intermediate temperatures the surface tension depends less strongly on temperature (near the knee in the curve shown in Fig. 4) and the adsorption is zero. Similar arguments can be used to show that positive Γ_B is reasonable at lower temperatures near the melting point of pure B.

IV. NONSTATIONARY INTERFACE

A. Governing equations for steady-state interface motion

We now consider a planar solid-liquid interface moving with a constant velocity V. Adopting a frame of reference translating at the same velocity and coincident with the center of the interfacial zone (given by $\phi = 1/2$ at $z = 0$ in this frame), the dimensional governing Eqs. (5) and (6) become

$$\varepsilon^2 \frac{d^2\phi}{dz^2} + \frac{V}{M_1}\frac{d\phi}{dz} - f_\phi = 0, \tag{43}$$

$$\frac{d}{dz}\left(c(1-c)\frac{d}{dz}\left[-\delta^2\frac{d^2c}{dz^2} + f_c\right]\right) + \frac{V}{M_2}\frac{dc}{dz} = 0. \tag{44}$$

with boundary conditions

$$\begin{aligned} &c \to c_{-\infty}, \quad \phi \to 1 \quad \text{as } z \to -\infty, \\ &c \to c_{+\infty}, \quad \phi \to 0 \quad \text{as } z \to +\infty, \end{aligned} \tag{45}$$

where $c_{+\infty}$ and $c_{-\infty}$ are the concentrations far from the interface in the liquid and solid respectively. Examination of these equations indicates that they include four associated length scales, given by

$$\ell_\varepsilon = \varepsilon\sqrt{\frac{v_m}{RT}}, \quad \ell_\delta = \delta\sqrt{\frac{v_m}{RT}},$$
$$\ell_{M_1} = \frac{V v_m}{M_1 RT}, \quad \ell_{M_2} = \frac{M_2 RT}{V v_m}. \tag{46}$$

The two length scales ℓ_ε and ℓ_δ arose in the case of the stationary interface discussed in the previous section, where ℓ_δ was chosen to nondimensionalize the governing equations. They are thus representative of the widths of the phase field and concentration fields in the interfacial zone, respectively, and are a result of the dependence of the Helmholtz free-energy functional $\mathcal{F}$ on their corresponding gradients. The two length scales ℓ_{M_1} and ℓ_{M_2} are directly associated with the motion of the interface. In particular, ℓ_{M_1} is associated with the dynamic response of the interface to nonequilibrium, and ℓ_{M_2}, on employing (8), is given by D/V, and is therefore the length scale on which the diffusive and advective transport balance in the standard diffusion models of solidification.

In this section we seek to extend the analysis of the stationary interface discussed in Sec. II to a nonstationary interface. As in the case of the stationary interface we choose ℓ_δ as our reference length scale by which to nondimensionalize the governing equations (43) and (44), which become

$$\tilde{\varepsilon}^2\frac{d^2\phi}{d\tilde{z}^2} + \tilde{\varepsilon}^2\frac{\tilde{V}}{\tilde{m}}\frac{d\phi}{d\tilde{z}} - \left[\tilde{f}_\phi^{(-2)}\tilde{\varepsilon}^{-2} + \tilde{f}_\phi^{(0)}\right] = 0, \tag{47}$$

$$\frac{d}{d\tilde{z}}\left\{c(1-c)\frac{d}{d\tilde{z}}\left[-\frac{d^2c}{d\tilde{z}^2} + \left(\tilde{f}_c^{(-2)}\tilde{\varepsilon}^{-2} + \tilde{f}_c^{(0)}\right)\right]\right\} + \frac{d^2c}{d\tilde{z}^2} + \tilde{V}\frac{dc}{d\tilde{z}} = 0, \tag{48}$$

where

$$\tilde{V} = \frac{V\ell_\delta}{D} \tag{49}$$

and

$$\tilde{m} = \frac{\ell_\varepsilon^2}{\ell_{M_1}\ell_{M_2}} = \frac{\varepsilon^2 M_1}{D} \tag{50}$$

are nondimensional representations of the interface velocity and mobility of the interface relative to that of solute, respectively. Here $z = \ell_\delta\tilde{z}$ and $\tilde{\varepsilon} = \varepsilon/\delta$, as defined earlier.

B. Governing equations for $\varepsilon/\delta \ll 1$

We have conducted an asymptotic analysis of the governing equations (47) and (48) in the limit $\tilde{\varepsilon} \to 0$, with the remaining parameters of order unity. In particular, the parameter $\tilde{m}$ may then be associated with interfacial kinetics; this requires that $\varepsilon^2 M_1$ is of order unity in this limit.

The details of the expansion are similar to those given in Sec. III, but the analysis is more complicated. For brevity we just state the results, which show that there is an layer of thickness $O(\tilde{\varepsilon}^2)$ about $\tilde{z} = 0$ where ϕ varies from zero to unity and c is constant at leading order. The leading-order solute field outside the interfacial layer satisfies the governing equation

$$\frac{d}{d\tilde{z}}\left(c(1-c)\frac{d}{d\tilde{z}}\left[-\frac{d^2c}{d\tilde{z}^2} + \tilde{f}_c^{(0)}\right]\right) + \frac{d^2c}{d\tilde{z}^2} + \tilde{V}\frac{dc}{d\tilde{z}} = 0, \tag{51}$$

with interfacial boundary conditions

$$c(0^+) = c(0^-) = \chi(\tilde{V}, T), \tag{52}$$

$$\left.\frac{dc}{d\tilde{z}}\right|_{\tilde{z}=0^-}^{\tilde{z}=0^+} = \Lambda, \tag{53}$$

$$\left.\frac{d^2c}{d\tilde{z}^2}\right|_{\tilde{z}=0^-}^{\tilde{z}=0^+} = \tilde{f}_c^{(0)}(0, \chi(\tilde{V}, T)) - \tilde{f}_c^{(0)}(1, \chi(\tilde{V}, T)), \tag{54}$$

$$\left.\frac{d^3c}{d\tilde{z}^3}\right|_{\tilde{z}=0^-}^{\tilde{z}=0^+} = \frac{\Lambda}{\chi(1-\chi)}, \tag{55}$$

and

$$c \to c_{+\infty} \quad \text{as} \quad \tilde{z} \to \infty \text{ and } c \to c_{-\infty} \quad \text{as} \quad \tilde{z} \to -\infty. \tag{56}$$

Here the interfacial concentration, $\chi(\tilde{V}, T)$, satisfies

$$\frac{\Lambda}{2}\left[\left.\frac{dc}{d\tilde{z}}\right|_{\tilde{z}=0^-} + \left.\frac{dc}{d\tilde{z}}\right|_{\tilde{z}=0^+}\right] + \frac{\tilde{V}}{\tilde{m}}\sqrt{\chi\tilde{\sigma}_B^2 + (1-\chi)\tilde{\sigma}_A^2} = \tilde{f}^{(0)}(0,\chi) - \tilde{f}^{(0)}(1,\chi). \tag{57}$$

We note that when the interface is stationary ($\tilde{V} = 0$), this reduces to the same expression (36) for $c^\star$ given in the previous section for the stationary interface. Using the above expression for pure A, we may relate $\tilde{m}$ to the dimensional interface kinetic coefficient for A, μ_A, as

$$\tilde{m} = \frac{\mu_A\sigma_A T_M^{(A)}}{L_A D}.$$

A similar expression can be obtained for pure B, but in general would lead to a different value for $\tilde{m}$. However, because we have assumed M_1 does not depend on composition, the values for μ_A and μ_B must be related, as described in Ref. [20]. Then the values for $\tilde{m}$ calculated for either pure A or pure B would be the same. Using the material parameters for the nickel-copper alloy given in WBM we find that $\tilde{m} \approx 500$. The fact that $\tilde{m}$ is large will play a role in the interpretation of the subsequent results. It should be emphasized that the dimensionless constants appearing in the above equations are then independent of ε, and can be computed solely from a knowledge of

conventional material parameters and δ.

The governing equation (51) and its associated boundary conditions (52), (53), (54), (55), and (56) provide a model for a continuous solute field across a structurally sharp interface located at $\tilde{z} = 0$, where the interfacial boundary conditions have been derived by taking the limit of the phase-field model as the interfacial thickness, ℓ_ε, becomes vanishingly small compared to the thickness of the solute layer, ℓ_δ. The boundary condition (52) represents continuity of the solute concentration at the interface, which arises because the transition layer in ϕ is much thinner than the length scale associated with the solute gradient energy in the limit $\tilde{\varepsilon} = \ell_\varepsilon/\ell_\delta \to 0$; this property was also observed for the stationary interface in the same limit $\tilde{\varepsilon} \to 0$. Boundary condition (54) in dimensional units states that the quantity $f_c - \delta^2 d^2c/dz^2$ is continuous across the interface. This quantity is $\delta\mathcal{F}/\delta c$, and is the generalized interdiffusion potential including the gradient-energy contributions [27]. The interdiffusion flux is proportional to $d(f_c - \delta^2 d^2c/dz^2)/dz$ and hence (53) and (55) taken together ensure that the interdiffusion flux is continuous across the interface, which, along with continuity of solute concentration there, ensures that the solute is conserved across the interface.

We integrate (51) once, which, on applying conservation of the solute across the interface and the far-field boundary conditions, yields

$$-c(1-c)\frac{d^3c}{d\tilde{z}^3} + \frac{dc}{d\tilde{z}} + \tilde{V}c = \tilde{V}c_\infty, \tag{58}$$

where the two far-field concentrations $c_{+\infty}$ and $c_{-\infty}$ must also be equal for this steady-state solution; their common value is denoted c_∞. The appropriate boundary conditions are (52), (53), and (54) at the interface $z = 0$; they may be written as

$$c(0^+) = c(0^-) = \chi(\tilde{V}, T), \tag{59}$$

$$\left.\frac{dc}{d\tilde{z}}\right|_{\tilde{z}=0^-}^{\tilde{z}=0^+} = \Lambda, \tag{60}$$

$$\left.\frac{d^2c}{d\tilde{z}^2}\right|_{\tilde{z}=0^-}^{\tilde{z}=0^+} = \widetilde{\Delta F}_A - \widetilde{\Delta F}_B. \tag{61}$$

The far-field boundary conditions are

$$c \to c_\infty \text{ as } |z| \to \infty. \tag{62}$$

As discussed in the previous section, Λ is small and we henceforth set it to zero, in which case (57) may be manipulated to show that the interfacial concentration $\chi(\tilde{V}, T)$ is given uniquely in terms of the interface velocity and system temperature by the root of

$$\chi^2\left[\widetilde{\Delta F}_B - \widetilde{\Delta F}_A\right]^2 + \chi\left[2\,\widetilde{\Delta F}_A\left(\widetilde{\Delta F}_B - \widetilde{\Delta F}_A\right) - \frac{\tilde{V}^2}{\tilde{m}^2}(\tilde{\sigma}_B^2 - \tilde{\sigma}_A^2)\right] + \left[(\widetilde{\Delta F}_A)^2 - \left(\frac{\tilde{V}\tilde{\sigma}_A}{\tilde{m}}\right)^2\right] = 0, \tag{63}$$

for which the right-hand side of (57) is positive. Further, we observe from Eq. (60) that in this case the first derivative of the concentration is continuous at the interface. All subsequent computations for the moving interface have been done with $\Lambda = 0$.

We now discuss the properties of the solute field given by the solution of (58)–(62) as the interface velocity increases. If for a given $\tilde{V}$, *both* the system temperature T and far-field concentration c_∞ are specified, then the boundary conditions overprescribe the problem, and in general a solution will not exist. However, if we only specify c_∞ and $\tilde{V}$ the above problem determines *both* the solute field and the system temperature, T. Below we first discuss the results of a numerical integration of the governing equations (58)–(62) and then proceed to interpret them in the light of further asymptotic analysis.

C. Numerical solution of the asymptotic governing equations

To investigate the dependence of the solute profile, $c(\tilde{z})$, and the system temperature, T, on the dimension-

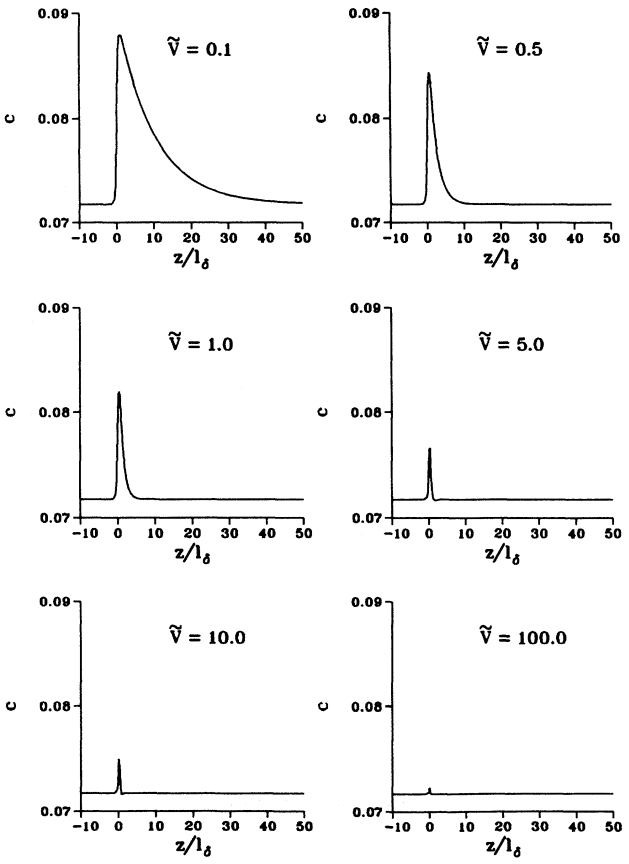

FIG. 5. The solute profile computed for different values of the dimensionless interface velocity $\tilde{V}$. Distance has been nondimensionalized with respect to ℓ_δ, which does not depend on the interface velocity. The material parameters are those for the nickel-copper alloy given by WBM and $\delta = 3.3 \times 10^{-4}$ J$^{1/2}$cm$^{-1/2}$.

less interface velocity, $\tilde{V}$, we have computed solutions of the governing equation (58) and its associated boundary conditions (59)–(62) using the NAG subroutine D02GAF [39], which employs a finite-difference discretization allied to Newton iteration. We performed computations for the case of the nickel-copper alloy for a range of values of $\tilde{V}$. The far-field concentration c_∞ was set to 7.17441×10^{-2}, which is the value of the solidus concentration at a temperature of 1700 K (see Fig. 1). Computations were performed using three values of δ given by $\delta = 3.3 \times 10^{-4}$ J$^{1/2}$cm$^{-1/2}$, 3.3×10^{-5} J$^{1/2}$cm$^{-1/2}$, and 3.3×10^{-6} J$^{1/2}$ cm$^{-1/2}$; the solute profiles, however, are not sensitive to the value of δ used, and for purposes of illustration we will show results for $\delta = 3.3 \times 10^{-4}$ J$^{1/2}$ cm$^{-1/2}$. The system temperature does depend strongly on the choice of δ, as we describe below.

In Figs. 5 and 6 we show the solute profiles for $\tilde{V} = 0.1, 0.5, 1.0, 5.0, 10.0$, and 100.0. In Fig. 5, the abscissa is z/ℓ_δ, which is proportional to physical distance and is independent of velocity. Figure 6 shows the same solute profiles but with distance scaled with respect to $\ell_{M_2} = D/V$, the conventional diffusion length. From Fig. 5 it is clear that the degree of segregation and the characteristic physical length of the solute field in the liquid ahead of the interfacial region ($z > 0$) monotonically decrease as the interface velocity increases. Although the length of the solute profile decreases, we see from Fig. 6 that it does not decrease as rapidly as the classical diffusion length, D/V.

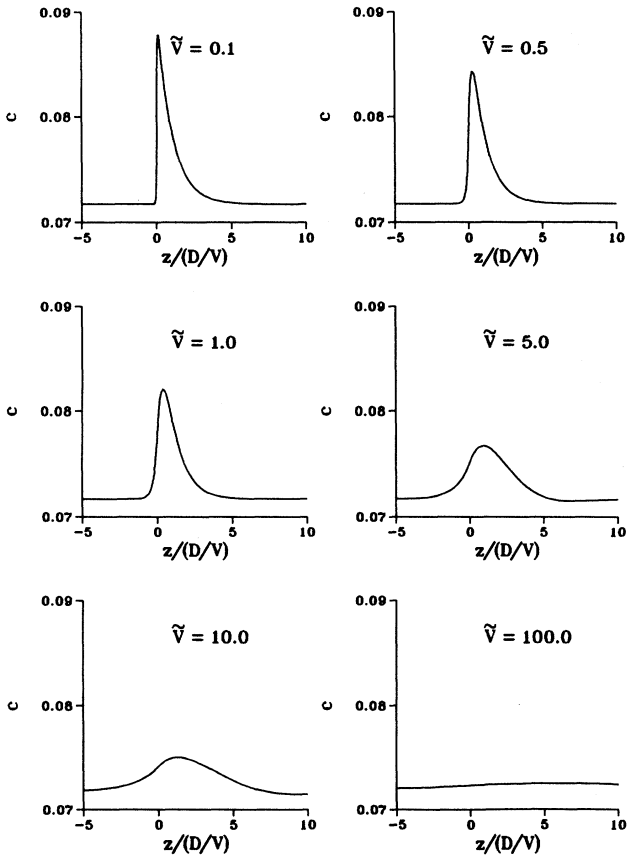

FIG. 6. The solute profile computed for different values of the dimensionless interface velocity $\tilde{V}$. Distance has been nondimensionalized with respect to the diffusion length, D/V. The material parameters are those for the nickel-copper alloy given by WBM and $\delta = 3.3 \times 10^{-4}$ J$^{1/2}$cm$^{-1/2}$.

In order to assess the dependence of the segregation on the interface velocity $\tilde{V}$ we computed the maximum value of $c(\tilde{z})$, denoted $c_{\max}$, and the interfacial concentration χ, as well as the corresponding temperature, T, for each value of $\tilde{V}$. In Figs. 7 and 8 we show the loci of the pairs $(c_{\max}, T)$ and (χ, T) superimposed on the phase diagram; these loci are parametrized by $\tilde{V}$. Results are shown for the same three values of δ given above. In all three cases, as the velocity increases, the value of $c_{\max}$ approaches the prescribed value $c_\infty = 7.174\,41 \times 10^{-2}$; this limiting case corresponds to partitionless solidification.

The rate of change of $c_{\max}$ with velocity is independent of the particular choice for δ, as can been seen by the vertical alignment of the solid circles on the curves in Fig. 7. On the other hand, the manner in which the temperature first increases and then decreases as $\tilde{V}$ is increased does depend strongly on δ.

D. Discussion of the numerical results

1. *Velocity-dependence of the solute profile*

At low velocities ($\tilde{V} \ll 1$) the degree of segregation in the liquid is greatest, with the maximum value of the

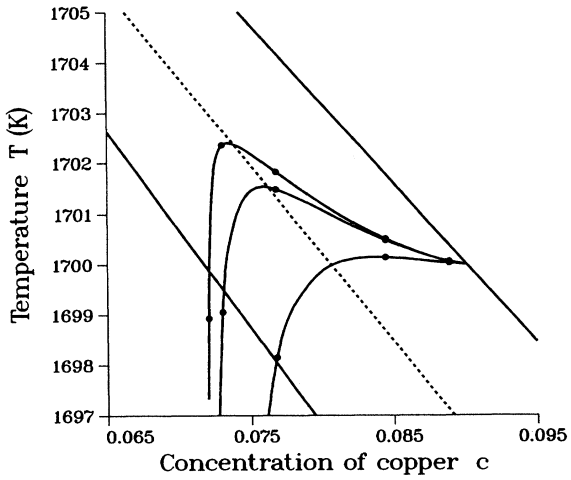

FIG. 7. An enlargement of the phase diagram given in Fig. 1. The upper and lower solid curves are the liquidus and solidus, respectively. The dashed curve is the locus of c^*. Also indicated by solid curves are the loci of the maximum concentrations, $c_{\max}$. These curves correspond (from top to bottom) to three values of $\delta = 3.3 \times 10^{-4}$ J$^{1/2}$cm$^{-1/2}$, 3.3×10^{-5} J$^{1/2}$cm$^{-1/2}$, and 3.3×10^{-6} J$^{1/2}$cm$^{-1/2}$. The solid circles on each curve represent (from right to left) data points corresponding to $\tilde{V} = 0.05$, 0.5, 5, 50, and 500. The data points for a given velocity are approximately aligned in the vertical direction, and some of the data points at high velocities are off-scale and not indicated in the figure.

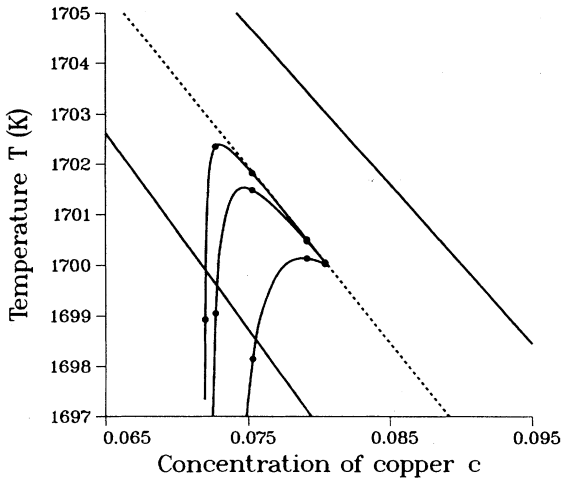

FIG. 8. An enlargement of the phase diagram given in Fig. 1. The upper and lower solid curves are the liquidus and solidus, respectively. The dashed curve is the locus of c^*. Also indicated by solid curves are the loci of the interfacial concentrations, χ. These curves correspond (from top to bottom) to three values of $\delta = 3.3 \times 10^{-4}$ J$^{1/2}$cm$^{-1/2}$, 3.3×10^{-5} J$^{1/2}$cm$^{-1/2}$, and 3.3×10^{-6} J$^{1/2}$cm$^{-1/2}$ The solid circles on each curve represent (from right to left) data points corresponding to $\tilde{V} = 0.05$, 0.5, 5, 50, and 500. The data points for a given velocity are approximately aligned in the vertical direction, and some of the data points at high velocities are off-scale and not indicated in the figure.

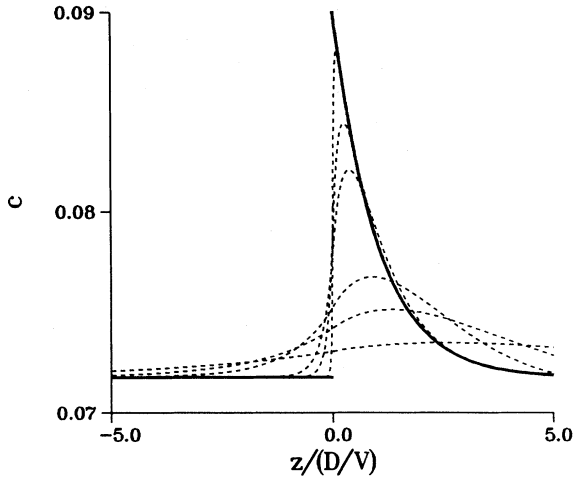

FIG. 9. The solid curve is the classical solute profile which is the leading-order solute profile as $\tilde{V} \to 0$. The dashed curves represent numerical solutions of (58)–(62) for different values of $\tilde{V}$ with $\delta = 3.3 \times 10^{-4}$ J$^{1/2}$ cm$^{-1/2}$. The dashed curves correspond to $\tilde{V} = 0.1$, 0.5, 1, 5, 10, and 30, in order of decreasing maxima.

concentration approaching the liquidus concentration as the interface velocity tends to zero. It is straightforward to conduct an asymptotic analysis of (58) and its boundary conditions in the limit $\tilde{V} \to 0$. This shows that a layer forms about the interface of thickness ℓ_δ which separates the two outer regions, one in the solid and one in the liquid. In the liquid outer region, the solute varies on the length scale, $\ell_{M_2} = D/V (\gg \ell_\delta)$. In the outer regions the solute concentration simply has, at leading order, the classical form associated with directional solidification of a planar interface:

$$c(\tilde{z}) = c_\infty + (c_L - c_\infty)\exp(-\tilde{V}\tilde{z}) \tag{64}$$

in the liquid region $\tilde{z} > 0$, and

$$c(\tilde{z}) = c_\infty \tag{65}$$

in the solid region $\tilde{z} < 0$. In the layer the concentration varies between the solidus concentration c_S in the solid phase and the liquidus c_L in the liquid phase, and the system temperature is given by the solidus temperature. In the outer regions the effect of the solute gradient energy is weak and only provides a regular perturbation to the classical exponential solute profile. However, in the layer centered on the interface the solute gradient energy is comparable to the Helmholtz free-energy density. In Fig. 9 we compare the computed profiles for $\delta = 3.3 \times 10^{-4}$ J$^{1/2}$cm$^{-1/2}$, some of which are plotted in Figs. 5 and 6, with the leading-order asymptotic solution (64) and (65). It clearly indicates that the classical result is achieved as $\tilde{V} \to 0^+$.

The length scale of the solute field diminishes monotonically as $\tilde{V}$ increases and the classical form of the solute field that is found at low interfacial velocities is disrupted at high velocities when its length scale D/V is comparable to the length scale of the interfacial layer, ℓ_δ, i.e., when $\tilde{V} \approx 1$. We also observe from the numerical calculations that at sufficiently large values of $\tilde{V}$ the solute field in the liquid develops a decaying oscillatory form. The solute profile in the far fields can be given explicitly by the expressions

$$c \sim c_\infty + A_1^\infty \exp(r_1\tilde{z}) + A_2^\infty \exp(r_2\tilde{z}), \tag{66}$$

in the liquid as $\tilde{z} \to +\infty$, and, in the solid,

$$c \sim c_\infty + A_3^\infty \exp(r_3\tilde{z}), \tag{67}$$

as $\tilde{z} \to -\infty$, where r_1, r_2, and r_3 are the three roots of the cubic

$$-c_\infty(1 - c_\infty)r^3 + r + \tilde{V} = 0. \tag{68}$$

The quantities r_1 and r_2 have negative real parts, and are either distinct and real, or are a complex conjugate pair; the third root r_3 is real and positive. The quantities A_1^∞ and A_2^∞ are two real or complex conjugate constants and A_3^∞ is a real constant.

When $\tilde{V}$ is small the roots of (68) are approximately given by

$$r_1 \approx -\sqrt{c_\infty(1 - c_\infty)}, \quad r_2 \approx -\tilde{V},$$

$$r_3 \approx +\sqrt{c_\infty(1 - c_\infty)},$$

and so the dominant contribution to the far-field concentration in the liquid is proportional to $\exp(-\tilde{V}\tilde{z})$ and the classical concentration profile (64) is recovered in the far field. From the formula for the roots of a cubic it may be shown that when $\tilde{V}^2 c_\infty(1-c_\infty) < 4/27$, all roots are real; otherwise, the roots r_1 and r_2 form a complex conjugate pair. Thus we expect a change in character of the concentration field in the liquid from monotonic decay at smaller velocities to a damped oscillation when the velocity is sufficiently large that

$$\tilde{V} > \frac{2}{3\sqrt{3c_\infty(1-c_\infty)}}.$$

We note that since r_3 is always real, there are no spatial oscillations in the solute profile in the solid. Further insight into the solution for large interface velocity can be obtained by conducting an asymptotic analysis of the governing equation (58) and its boundary conditions in the limit $\tilde{V} \to \infty$, which shows that, in the liquid $\bar{z} > 0$,

$$c \sim c_\infty + \tilde{V}^{-2/3}\beta \exp\left(-\frac{\bar{z}}{2}\right)\cos\left(\frac{\bar{z}\sqrt{3}}{2} - \frac{\pi}{3}\right) + O(\tilde{V}^{-1}), \tag{69}$$

and, in the solid $\bar{z} < 0$,

$$c \sim c_\infty + \tilde{V}^{-2/3}\frac{\beta}{2}\exp(\bar{z}), \tag{70}$$

where

$$\beta = \frac{2v_m[c_\infty(1-c_\infty)]^{2/3}}{3RT}\left[L_B\frac{T-T_M^{(B)}}{T_M^{(B)}} - L_A\frac{T-T_M^{(A)}}{T_M^{(A)}}\right], \tag{71}$$

and $\tilde{z} = \bar{z}[c_\infty(1-c_\infty)/\tilde{V}]^{1/3}$. Thus at high interface velocities the characteristic length of the solute profile is $\ell_\delta \tilde{V}^{-1/3} = (\ell_\delta^2 \ell_{M_2})^{1/3}$, and in the liquid the profile has damped oscillations, as indeed are observed in the computations (see Fig. 10). Thus, the length scale of the solute field, although becoming smaller with increasing interface velocity, is much larger than would be expected on the basis of the diffusion length $\ell_{M_2} = D/V = \ell_\delta/\tilde{V}$ alone, as suggested by our calculations displayed in Fig. 6. Moreover, we note that $(c_{\max} - c_{\min})$ decreases like $\tilde{V}^{-2/3}$ for large interface velocities. In Fig. 10 we compare the computed solution of Eq. (58) with the asymptotic forms (69) and (70) for $\tilde{V} \to \infty$, and show increasingly good agreement as $\tilde{V}$ increases.

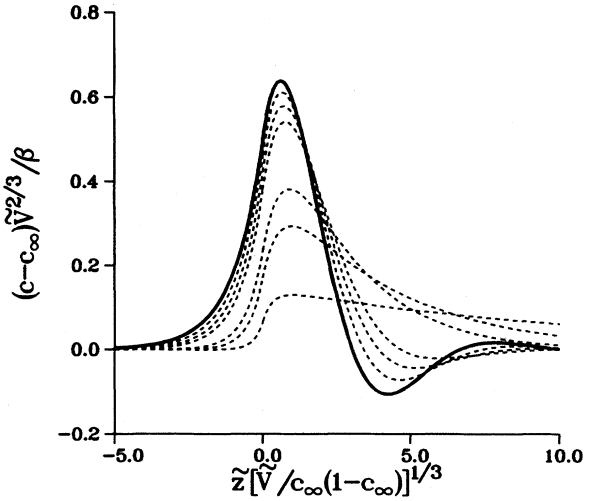

FIG. 10. A comparison of the computed concentration profiles for $\delta = 3.3 \times 10^{-4}$ J$^{1/2}$cm$^{-1/2}$ displayed in Figs. 5 and 6 for different values of $\tilde{V}$ (given by the dashed curves) with the asymptotic forms (69) and (70) (given by the solid curve) corresponding to the limit $\tilde{V} \to \infty$. The computed profiles correspond to $\tilde{V} = 0.1$, 0.5, 1, 5, 10, and 30 in order of increasing maxima.

2. *Velocity dependence of system temperature*

We now discuss the dependence of the system temperature on the interface velocity, under the assumption that Λ is zero. As seen in Fig. 7, as $\tilde{V}$ increases from zero the system temperature initially increases. The temperature rise is greater for large values of δ. This effect is due to the size of the second term on the left-hand side of (57). The value of $\tilde{m} \approx 500$ is large. When $\tilde{V}/\tilde{m}$ is small, this term is small and may be approximated by zero, in which case the interfacial concentration is well approximated by $\chi(T) = c^*(T)$. As $\tilde{V}$ increases, the interfacial concentration decreases due to the presence of the solute gradient energy. This requires the temperature to increase because c^* is a monotonic decreasing function of the temperature; see Fig. 1. Over the range of velocities for which $\tilde{V}/\tilde{m}$ is small, $\tilde{V}$ may become large, and the concentration at the interface changes from its value for a stationary interface to approximately c_∞. It is this range of interface velocities which characterizes the transition to partitionless growth. A further increase in the interface velocity to values for which $\tilde{V}/\tilde{m}$ is not small results in very little further change in the interfacial concentration. Thus, from (57) the temperature decreases linearly with increasing velocity, which is the result of interface kinetics (the mobility M_1). The value of δ affects the range of values of $\tilde{V}$ over which the initial temperature rise occurs because of the factor $\sqrt{\chi\tilde{\sigma}_A^2 + (1-\chi)\tilde{\sigma}_B^2}$ in the left-hand side of (57), which is inversely proportional to δ.

In summary, the effect of increasing the interface velocity on the solute profile is to cause a progressive reduction of its characteristic length scale, from $\ell_\delta \tilde{V}^{-1} = D/V$, when $\tilde{V}$ is small, to $\ell_\delta \tilde{V}^{-1/3}$ at large values of $\tilde{V}$. In making this transition, the form of the solute field in the liquid develops a damped oscillation. The maximum value of the concentration, and hence the segregation, decreases monotonically as the interface velocity is increased. Over the range of values of $\tilde{V}$ for which the segregation is reduced, the system temperature increases. Further increase in the interface velocity results in the temperature decreasing linearly with velocity, similar to the effects of linear interface kinetics in a pure material.

V. DISCUSSION

In the previous sections we have presented and analyzed a model of solute trapping. In particular we have considered the properties of the solution to this model in the limit $\varepsilon/\delta \to 0$. This we believe is the appropriate limit because the variation of concentration across an interface is thought to occur on a length scale longer than the associated change in atomic order, which here is represented by the phase field. We have shown that by taking this limit of our phase model we may recover a new model of solute trapping in which the interface is structurally sharp. This new model is independent of the value of the phase-field gradient-energy coefficient ε, and is completely specified by the conventional material and growth parameters and the value of the solute gradient-energy coefficient. While the latter quantity does not appear in classical models of solidification, our analysis indicates that it may be experimentally determined from a knowledge of the dependence of the interfacial surface tension on temperature, and thus concentration, or, as we show below, from the dependence of the partition coefficient on the interface velocity.

In the absence of the solute gradient energy, the solute field is given by the exponential profile (64), with the associated length scale $\ell_{M_2} = D/V$, which has the property that $\ell_{M_2} \to 0$ as $V \to \infty$. Employing $D = 10^{-5}$ $\mathrm{cm^2\ s^{-1}}$ as a typical value of the diffusion coefficient of a binary alloy, it is clear that for values of the interface velocity in excess of approximately 1 $\mathrm{m\ s^{-1}}$, ℓ_{M_2} is on the order of the atomic scale. Such large velocities are commonly encountered in rapid solidification, and applying a model based on a classical solute diffusion equation on such a small length scale is therefore an important issue. In the model presented here the solute gradient energy acts to oppose the contraction of the length scale associated with large velocities. Indeed for velocities where $\tilde{V}$ is large the analysis given in Sec. III shows that the length scale of the solute profile is $\ell_\delta \tilde{V}^{-1/3}$. This length scale in dimensional units, denoted by ℓ_∞, is given as

$$\ell_\infty = \left(\frac{\delta^2 D v_m}{VRT}\right)^{1/3}. \tag{72}$$

Employing the data for the nickel-copper alloy given in WBM, we find $\ell_\infty \approx 6 \times 10^{-3}(\delta^2 V)^{1/3}$ cm, where δ and V have units of $\mathrm{J^{1/2}cm^{-1/2}}$ and $\mathrm{cm\ s^{-1}}$, respectively, in which case $\ell_\infty > 10^{-8}$ cm (typical of atomic dimensions) providing that $V < 10^{16}\delta^2$ $\mathrm{cm\ s^{-1}}$. Assuming $\delta > 10^{-5}$ $\mathrm{J^{1/2}\ cm^{-1/2}}$, our asymptotic model should be valid for interfacial velocities up to 1 $\mathrm{km\ s^{-1}}$, which surpasses the limitation of 1 $\mathrm{m\ s^{-1}}$ required of earlier models that employ the diffusion equation without solute gradient-energy terms.

In our asymptotic model, we find that the concentration is continuous across the interface and that the concentration field is described by (58) and boundary conditions (59)–(62). In the limit $\tilde{V} \to 0$, appropriate to low interface velocities, a thin solute layer of size ℓ_δ forms across the interface in which the concentration varies rapidly. The concentrations at each side of this layer, in the solid and liquid, are given by the common tangent construction at small interface velocities, and so there is effectively a jump in the concentration across this thin layer at the interface. However for general values of the interface velocity the concentration is continuous and we are not able to define the partition coefficient in the conventional manner. To facilitate comparison of our results to sharp-interface models of solute trapping, and only for that reason, we define a quantity $k^\star$ as

$$k^\star = \frac{\text{(far-field concentration)}}{\text{(maximum value of the concentration)}}. \tag{73}$$

The analysis for low velocities indicates that $k^\star \to k_e$ as $\tilde{V} \to 0$, where k_e is the conventionally defined equilibrium partition coefficient. In Fig. 11 we plot $k^\star$ from our computations of the solute profile as a function of the interface velocity $\tilde{V}$.

It appears from our computations that the maximum value of the concentration decreases and hence $k^\star$ increases as the interface velocity increases. At sufficiently high velocities the concentration is approximately uniform everywhere and equal to its far-field value, and so $k^\star$ will approach unity from below as the interface velocity becomes infinite. In fact from the form of the solution obtained in the limit of large interface velocity given by (69) and (70) for $\Lambda = 0$ it can be shown that

$$k^\star = 1 - \kappa \tilde{V}^{-2/3} + O(\tilde{V}^{-1}), \tag{74}$$

where $\kappa = \gamma\beta/c_\infty$ and $\gamma = \sqrt{3}\exp[-\pi/(3\sqrt{3})]/2 \approx 0.47$. The quantity β is given by (71), and after substitution into (74), the first two terms give the dimensional form

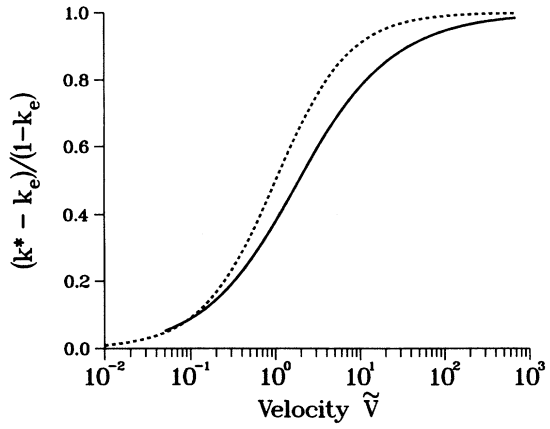

FIG. 11. The normalized quantity $(k^\star - k_e)/(1 - k_e)$, calculated from our computations, plotted against the interface velocity $\tilde{V}$, for the case of the nickel-copper alloy with $\delta = 3.3 \times 10^{-4}$ $\mathrm{J^{1/2}cm^{-1/2}}$, $\delta = 3.3 \times 10^{-5}$ $\mathrm{J^{1/2}cm^{-1/2}}$, and 3.3×10^{-6} $\mathrm{J^{1/2}cm^{-1/2}}$. The solid curve superimposes the predictions for the three values of δ and are essentially indistinguishable. The dashed curve represents the form of the the dependence used in the Aziz theory; $k = (k_e + \tilde{V})/(1 + \tilde{V})$; here k_e is the value of the partition coefficient for a stationary interface, which for the nickel-copper alloy at 1700 K is 0.8.

for $k^\star$ as

$$k^\star \approx 1 - \frac{2\gamma}{3(c_\infty)^{1/3}} \left(\frac{D(1-c_\infty)}{V\delta}\right)^{2/3} \times \left(\frac{v_m}{RT}\right)^{2/3} \left[L_B \frac{T - T_M^{(B)}}{T_M^{(B)}} - L_A \frac{T - T_M^{(A)}}{T_M^{(A)}}\right], \tag{75}$$

for large interface velocities. In this expression the temperature T can be obtained from Eq. (57), with $\Lambda = 0$ to be consistent with the assumption used in the numerical computations. One might note that in the limit of infinitely fast interface kinetics, $\tilde{m} \to \infty$, the following expression for the system temperature is obtained at leading order:

$$T = T_M^{(A)} T_M^{(B)} \left[\frac{(1-c_\infty)L_A + c_\infty L_B}{(1-c_\infty)L_A T_M^{(B)} + c_\infty L_B T_M^{(A)}}\right].$$

This is the equation for the T_0 curve.

The present results can be compared to a sharp-interface model commonly used to describe the interface partition coefficient and the interface temperature. This comparison is only made for the purpose of illustration and is artificial in the sense that the present model and sharp-interface models of solute trapping are fundamentally different. For dilute alloys the functional form of k, the ratio of the liquid and solid compositions at a sharp interface, can be given by [8, 40]

$$k = \frac{k_e + V/V_D}{1 + V/V_D},$$

where k_e is the equilibrium partition coefficient, and V_D is a characteristic kinetic velocity for solute trapping, which is often taken as D_i/a_0, with D_i a diffusion coefficient in the interface and a_0 an interatomic dimension.

Two formulations for the dependence of interface temperature on velocity associated with this sharp-interface model have been obtained by Aziz and Kaplan [28], depending on whether or not solute drag [41] is included in the dissipation of the free-energy difference that drives solidification. For dilute alloys with a fixed solid composition, c_∞, the temperature is given by

$$T = T_M + \frac{m_L c_\infty}{k}\left(\frac{1 - k + \alpha \ln(k/k_e)}{1 - k_e}\right) - \frac{V}{\mu}, \tag{76}$$

where T_M is the pure (solvent) melting point, m_L is the slope of the liquidus, and μ is the interface kinetic coefficient for the pure solvent. The parameter α is equal to k when solute drag is neglected [42, 43] and equal to unity when solute drag is included [44].

Figures 11–13 compare the results of the present investigation with the above sharp interface models by equating the dimensionless velocities $\tilde{V}$ and V/V_D. [Equating these velocities gives the value $\delta = \sqrt{RT/v_m}(D/V_D)$.] Values for T_M, m_L, and k_e were taken from the data of Fig. 1 and the value for μ was chosen as 200 cm K^{-1} s^{-1} (corresponding to a value for M_1 of 4.9×10^8 cm^3 J^{-1} s^{-1} [20]).

In Fig. 11, the two curves showing the velocity dependence of k and $k^\star$ are remarkably similar. From this similarity one can extract a value of δ which agrees with data on solute trapping obtained from experiments using pulsed lasers to rapidly melt and resolidification thin layers of alloys and ion-implanted Si. These experiments give values for V_D on the order of 10 m s^{-1} [21–23]. One might estimate the same value for the character-

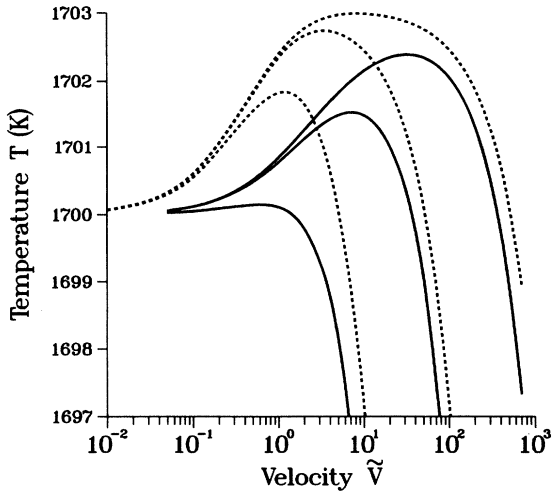

FIG. 12. The solid curves show computed system temperature, T, as a function of the interface velocity, $\tilde{V}$ for (from top to bottom) $\delta = 3.3 \times 10^{-4}$ J$^{1/2}$cm$^{-1/2}$, 3.3×10^{-5} J$^{1/2}$cm$^{-1/2}$, and 3.3×10^{-6} J$^{1/2}$cm$^{-1/2}$. The dashed curve associated with each solid curve represents the corresponding temperature dependence upon the interface velocity based on a sharp interface theory without solute drag [28] [$\alpha = k$ in Eq. (76)].

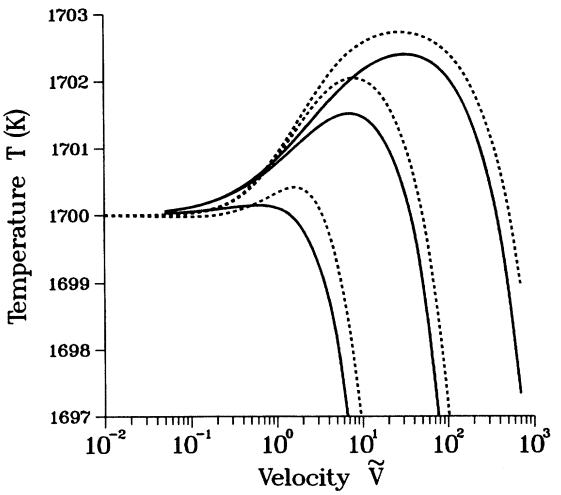

FIG. 13. The solid curves show computed system temperature, T, as a function of the interface velocity, $\tilde{V}$ for (from top to bottom) $\delta = 3.3 \times 10^{-4}$ J$^{1/2}$cm$^{-1/2}$, 3.3×10^{-5} J$^{1/2}$cm$^{-1/2}$, and 3.3×10^{-6} J$^{1/2}$cm$^{-1/2}$. The dashed curve associated with each solid curve represents the corresponding temperature dependence upon the interface velocity based on a sharp interface theory with solute drag [44] [$\alpha = 1$ in Eq. (76)].

istic trapping velocity, D/ℓ_δ, from the phase-field model. In this manner, values of $\ell_\delta = 10^{-8}$ cm or $\delta = 4.2 \times 10^{-7}$ $J^{1/2}$ $cm^{-1/2}$ can be obtained. This value is significantly smaller than that used in the present calculations. Since the experimental determination of V_D was obtained using solutions to the classical diffusion equation, it would be interesting to reinterpret the raw data of solute trapping experiments using the current asymptotic model to determine values of δ. However, this reinterpretation would require the solution of the diffusion equation with the contribution of the solute gradient-energy coefficient included.

In Figs. 12 and 13 we show the comparison of the dependence of the temperature on velocity obtained in the phase-field model to the sharp-interface model without and with solute drag, respectively. The temperature predictions of the present model more closely resemble the sharp-interface model in which the dissipation of free energy due to solute drag is included. This similarity may be due to the fact that the phase-field model naturally includes the presence of surface excesses and their transport with the moving interfacial zone during solidification.

VI. CONCLUSION

The description of solute trapping using a phase-field model with solute gradient-energy terms is intuitively appealing. With equilibrium partioning, the solute gradients in the liquid near the interface become increasingly severe at high solidification rates. It is natural to suppose that for large enough velocities, the energy required to maintain the solute gradient becomes too high, and instead equilibrium partitioning of the solute at the interface is abandoned in order that less severe gradients can be maintained. The phase-field model described here provides a mechanism for the realization of these intuitive concepts: large solute gradients in the system are penalized by the inclusion of the solute gradient-energy term in the free-energy functional. Kinetic equations based on variational derivatives of this free-energy functional then provide a consistent framework for the evolution of the system under nonequilibrium conditions.

The governing equations described here are based on an ideal solution model of the bulk phases, allowing the modeling of simple systems with lens-shaped phase diagrams. In addition to the classical materials parameters associated with alloy solidification, our model requires the specification of two other parameters that appear as coefficients of the gradients of the phase field and concentration field in the free-energy functional. The governing equations then exhibit two additional lengths scales determined by the gradient-energy coefficients, each characterize the width of diffuse transition layers of these fields. For an isothermal system with a stationary planar geometry, these are the only lengths in the system and, in the bulk regions outside of the transition layers, the solute field in each phase is uniform and given by the equilibrium values consistent with the temperature of the system. For systems with a steadily propagating solidification front, however, we find that deviations from equilibrium behavior occur, leading to solute trapping at high velocities.

We have argued that near the solidification front, the length scale associated with the transition layer of the phase field is small compared to the more diffuse transition for the solute field. This scaling defines an asymptotic regime in which the phase-field gradient-energy terms can be neglected, while the solute gradient-energy terms are retained. The asymptotic governing equations obtained in this limit have the advantage that the phase field no longer appears. The transition in passing from the solid region to the liquid region is then spatially sharp, and appropriate jump conditions across this surface are derived for the fourth-order solute-diffusion equation. In particular, we find that the solute field is continuous across the interphase boundary, but for comparison to sharp-interface models we define an effective partition coefficient $k^\star$. We employ a reasonable definition based on the ratio between the solid concentration far from the interface and the maximum liquid concentration. This quantity reduces to the usual definition at low velocities.

We have studied the solutions to the asymptotic equations both numerically, for a range of solidification velocities, and asymptotically, in the limits of high and low velocities. At low velocities, in the regions far from the interface, the steady-state solute profiles approach the familiar exponential distributions obtained from the classical diffusion equation, and the profiles exhibit the characteristic length D/V based on the ratio of the solute diffusivity and the solidification velocity. The solute concentrations near the interface satisfy equilibrium partitioning. Although the phase boundary is structurally sharp in this model, at low velocities there is still a transition region of rapid solute variation near the phase boundary associated with the solute gradient-energy term. As the velocity is increased and the length scale D/V becomes comparable to that of the solute gradient-energy term, the length scale of the solute field changes from D/V to a relatively longer scale given by a geometric mean of these two length scales. As this occurs, the concentration becomes uniform. In particular, the deviation of $k^\star$ from unity is found to decrease as $V^{-2/3}$ as the solidification velocity is increased. At high velocities, the solute profile in the liquid is not monotonic, but is found to exhibit a spatial oscillation that produces concentrations in the liquid that lie below the far-field concentration. This profile is a direct result of the fourth-order diffusion equation, and is not observed for the classical second-order diffusion equation.

The theory also suggests possible means for the experimental determination of the solute gradient-energy coefficient, which is a quantity that is not contained in the usual database of materials parameters.

We have compared the predicted dependence on solidification velocity of the solute partitioning and system temperature obtained by using the phase-field model with the predictions of two other popular models based on atomistic descriptions of solute partitioning at a moving interface. If the parameters in the respective models are identified in an appropriate manner, the predictions

of the phase-field model are found to be in qualitative agreement with one of the other two models that includes the effects of solute drag.

While the asymptotic limit considered here does clarify the mechanism of solute trapping at high solidification rates, it has the disadvantage that a surface of discontinuity is reintroduced across which jumps in the higher derivatives of the solute field must be specified. For the purposes of numerical computation in more than one dimension, it is preferable to revert to the full set of governing equations.

It would be of interest to employ the predictions of the fourth-order diffusion equation discussed here to aid in the interpretation of experimental data for solute trapping. Extending the theory to more complex geometries and to nonisothermal alloys are also important areas of research. Other extensions of the theory would allow the treatment of more complicated binary alloys, such as eutectic systems.

ACKNOWLEDGMENTS

The authors are grateful for discussions with R. J Braun, J. W. Cahn, S. R. Coriell, S. H. Davis, and B. T. Murray. A.A.W. and G.B.M. acknowledge support from a NATO collaborative grant, and the Applied and Computational Mathematics Program of DARPA. G.B.M. also acknowledges support from the Microgravity Science and Applications Program of NASA. A portion of the work was performed while one of the authors (G.B.M.) was visiting the Department of Engineering Sciences and Applied Mathematics, Northwestern University, whose hospitality is gratefully acknowledged.

* Permanent address: School of Mathematics, University of Bristol, BS8 1TW, United Kingdom.

[1] J. C. Baker, Ph.D thesis, MIT, 1970 (unpublished).
[2] J. S. Langer and R. F. Sekerka, Acta Metall. **23**, 1225 (1975).
[3] A. A. Chernov,Usp. Fiz. Nauk **100**, 277 (1970) [Sov. Phys. Usp. **13**, 101 (1970)].
[4] K. A. Jackson, in *Surface Modification and Alloying by Laser Ion and Electron Beams*, edited by J. M. Poate, G. Foti, and D. C. Jacobson (Plenum, New York, 1983), p. 62.
[5] G. H. Gilmer, Mater. Res. Soc. Symp. Proc. **13**, 249 (1983).
[6] H. Pfeiffer, Phys. Stat. Solidi A **99**, 139 (1980).
[7] D. E. Temkin, Kristallografiya **17**, 461 (1972) [Sov. Phys. Crystallogr. **17**, 405 (1972)].
[8] M. J. Aziz, J. Appl. Phys. **53**, 1158 (1982).
[9] S. R. Coriell and D. Turnbull, Acta Metall. **30**, 135 (1970).
[10] C. MacDonald, A. M. Malvezzi, and F. Spaepen, J. Appl. Phys **65**, 129 (1988).
[11] J. Q. Broughton, G. H. Gilmer, and K. A. Jackson, Phys. Rev. Lett. **49**, 1946 (1982).
[12] J. S. Langer (unpublished).
[13] J. S. Langer, in *Directions in Condensed Matter Physics*, edited by G. Grinstein and G. Mazenko (World Scientific, Philadelphia, 1986), pp. 164–186.
[14] G. Caginalp, Department of Mathematics Technical Report No. 82-5, Carnegie Mellon University, 1982 (unpublished).
[15] J. B. Collins and H. Levine, Phys. Rev. B **31**, 6119 (1985).
[16] G. Caginalp, in *Applications of Field Theory to Statistical Mechanics*, edited by Luis Garrido, Lecture Notes in Physics No. 216 (Springer-Verlag, Berlin, 1984), pp. 216–226.
[17] G. Caginalp, Arch. Rat. Mech. Anal. **92**, 205 (1986).
[18] P. C. Fife, in *Proceedings of the Taniguchi International Symposium on Nonlinear PDES and Applications* (Kinokuniya, Tokyo, 1990).
[19] H. Lowen, J. Bechoefer, and L. S. Tuckerman, Phys. Rev. A **45**, 2399 (1992).
[20] A. A. Wheeler, W. J. Boettinger, and G. B. McFadden, Phys. Rev. A **45**, 7424 (1992).
[21] M. J. Aziz, J. Y. Tsao, M. O. Thomson, P. S. Peercy, and C. W. White, Phys. Rev. Lett. **56**, 2489 (1986).
[22] M. J. Aziz and C. W. White, Phys. Rev. Lett. **57**, 2675 (1986).
[23] P. M. Smith, Ph.D thesis, Harvard University, 1992 (unpublished).
[24] H. E. Cook and J. E. Hilliard, J. Appl. Phys. **40**, 2191 (1969).
[25] T. Tsakalakos, Acta Metall. **33**, 1939 (1985).
[26] P. Dugan and T. Tsakalakos, Mater. Sci. Eng. B **6**, 171 (1990).
[27] J. E. Hilliard, in *Phase Transformations* (American Society For Metals, Metals Park, OH, 1970), pp. 497–560.
[28] M. J. Aziz and T. Kaplan, Acta Metall. **8**, 2335 (1988).
[29] R. Kobayashi, Physica D (to be published).
[30] S. Allen and J. W. Cahn, Acta Metall. **27**, 1085 (1979).
[31] J. W. Cahn and J. E. Hilliard, J. Chem. Phys. **28**, 258 (1958).
[32] J. W. Cahn, Acta Metall. **9**, 795 (1961).
[33] J. C. Baker and J. W. Cahn, in *Solidification* (American Society for Metals, Metals Park, Ohio, 1970).
[34] J. W. Gibbs, *Thermodynamics, Vol. 1* (Yale University Press, New Haven, 1948).
[35] C. H. P. Lupis, *Classical Thermodynamics of Materials* (North-Holland, Amsterdam, 1983).
[36] J. W. Cahn, J. Chem. Phys. **66**, 3667 (1977).
[37] A. Passerone, N. Eustathopolis, and P. Desre, J. Less-Common Met. **52**, 37 (1977).
[38] N. Eustathopolis, Int. Met. Rev. **28**, 189 (1983).
[39] B. Ford and J. C. T. Pool, in *Sources and Development of Mathematical Software*, edited by W. R. Cowell (Prentice-Hall, Englewood Cliffs, NJ, 1984), pp. 375–398.
[40] K. A. Jackson, G. H. Gilmer, and H. J. Leamy, in *Laser and Electron Beam Processing of Materials*, edited by C. W. White and P. S. Peercy, (Academic, New York, 1980), p. 104.
[41] J. W. Cahn, Acta Metall. **10**, 789 (1962).
[42] W. J. Boettinger and S. R. Coriell, in *Science and Technology of the Undercooled Melt*, edited by P. R. Sahm, H. Jones, and C. M. Adam (Nijhoff, Dordrecht, 1986), pp. 81–108.
[43] W. J. Boettinger, S. R. Coriell, and R. Trivedi, in *Rapid Solidification: Principles and Technologies* (Claitor's, Baton-Rouge, LA, 1988), pp. 13–25.
[44] M. J. Aziz and W. J. Boettinger (unpublished).